20th International Conference on Information Fusion
Xi'an, China - July 10-13, 2017

Projection-Based Circular Constrained State Estimation and Fusion Over Long-Haul Links

Qiang Liu and Nageswara S. V. Rao
Computational Sciences and Engineering Division
Oak Ridge National Laboratory
Oak Ridge, TN 37831
Email: {liuq1,raons}@ornl.gov

***Abstract*—In this paper, we consider a scenario where sensors are deployed over a large geographical area for tracking a target with circular nonlinear constraints on its motion dynamics. The sensor state estimates are sent over long-haul networks to a remote fusion center for fusion. We are interested in different ways to incorporate the constraints into the estimation and fusion process in the presence of communication loss. In particular, we consider closed-form projection-based solutions, including rules for fusing the estimates and for incorporating the constraints, which jointly can guarantee timely fusion often required in real-time systems. We test the performance of these methods in the long-haul tracking environment using a simple example.**

***Index Terms*—Long-haul sensor networks, state estimate fusion, error covariance matrices, nonlinear constraints, circular track constraints, root-mean-square-error (RMSE) performance, projection method.**

I. Introduction

In long-haul sensor networks, ground, airborne, or underwater sensors with sensing, data processing, and communication capabilities are deployed for tasks such as target tracking/monitoring to support military operations, national security, and environmental monitoring [1], [3]. The long-haul links between the sensor and the remote fusion center can be fiber-optic, satellite, or underwater acoustic links that span long distances to cover a very large geographical area. Typically, the target state estimates and the associated error covariances generated by the sensors are sent to the fusion center that fuses the data to obtain global estimates periodically at specified time instants. Fusion is a viable means to aggregate information from multiple sources and improve the overall tracking accuracy. However, the long propagation time and sporadic/bursty losses over the long-haul connection can effectively reduce the amount of useful data available at the fusion center, leading to degraded fusion performance and even failure to meet the system requirements on the overall quality of fused estimates.

In addition, in many ground target tracking applications, target dynamics are subject to certain constraints such as those defined by roadways. There have been a number of studies addressing constrained estimation problems, often in the context of Kalman filtering. A unifying modeling framework for equality-constrained dynamic systems is proposed in [18] using a distance-based optimization criterion. Target state-space modeling accounting for constraints has been studied in [4] and [5] respectively for straight-line and circular tracks. On the other hand, constrained fusion has received much less attention. [6] appears to be the most relevant work in this domain, where constrained fusion is studied in the context of centralized and distributed incorporation of known linear constraints, and in particular, [9] and [10] have considered linear constrained fusion in the context of information loss.

Our earlier studies have proposed various approaches to tackle the incomplete state estimate information at the fusion center, notably via information-driven selected fusion [13], message-level retransmission and retrodiction [14], staggered sensing scheduling [11], information feedback [12], and learning-based fusion [8]. This work continues our investigation of constrained fusion with information loss, but it focuses on quadratic constraints such as those characterized by circular tracks. The nonlinearity specified in the constraint (and the underlying state model) entails increased complexity for the overall estimation and fusion process. Of special interest to us are closed-form solutions for both the sensors and the fusion center to generate the state estimates with minimal computational overhead. We are particularly interested in exploring the joint effect of various (i) projection techniques to incorporate the constraints into the estimation process at the sensors and/or the fusion center; (ii) fusion rules; and (iii) ways in which the fusion center handles missing sensor estimates on fusion performance. A tracking example is used to demonstrate the performance of these constrained estimation and fusion approaches. Results show that by incorporating the circular constraint using the projection method, the fusion center can effectively improve the overall tracking accuracy under various loss conditions.

The rest of the paper is organized as follows: Section II provides an overview of linear constrained estimation and in particular, the projection method to incorporate the constraint. Section III focuses on nonlinear constrained estimation where the constraint is in the form of a circle with known center and radius. Both the first- and second-order solutions are presented. In Section IV, we discuss methods to combine these constrained estimates at the fusion center with existing closed-form fusion rules. A simulation example is used in Section V to demonstrate the joint effect of variable information loss, ways to perform projection, and fuser types on tracking performance before we conclude the paper in Section VI.

978-0-9964-5270-0©2017 ISIF

II. LINEAR CONSTRAINED ESTIMATION AND PROJECTION

In this section, we briefly review linear constrained estimation, and specifically, the projection method.

A. Continuous White-Noise Acceleration (CWNA) Model

As a commonly used straight-line motion model, the discretized continuous white noise acceleration model assumes an object travels in a generic coordinate at a near constant speed. Consider a 2D tracking scenario with orthogonal coordinates ξ and η. The evolution of the state vector $\mathbf{x} = [\xi \quad \dot{\xi} \quad \eta \quad \dot{\eta}]^T$ is described as

$$\mathbf{x}_{k+1} = \mathbf{F}\mathbf{x}_k + \mathbf{u}_k = \begin{bmatrix} \begin{bmatrix} 1 & T \\ 0 & 1 \end{bmatrix} & \mathbf{0}_{2\times 2} \\ \mathbf{0}_{2\times 2} & \begin{bmatrix} 1 & T \\ 0 & 1 \end{bmatrix} \end{bmatrix} \mathbf{x}_k + \mathbf{u}_k, \tag{1}$$

where the state estimate $\mathbf{x}$ is composed of position and velocity components along both axes, $\mathbf{F}$ is the state transition matrix, T is the sampling period[1], the subscript k is the discrete time index, and $\mathbf{u}_k$ is the process noise whose covariance matrix is given by

$$\mathbf{Q} = \begin{bmatrix} \tilde{q}_\xi \begin{bmatrix} T^3/3 & T^2/2 \\ T^2/2 & T \end{bmatrix} & \mathbf{0}_{2\times 2} \\ \mathbf{0}_{2\times 2} & \tilde{q}_\eta \begin{bmatrix} T^3/3 & T^2/2 \\ T^2/2 & T \end{bmatrix} \end{bmatrix}, \tag{2}$$

in which $\tilde{q}_\xi$ and $\tilde{q}_\eta$ (often assumed to be constant over time) are the power spectral densities (PSDs) of the underlying continuous-time white stochastic process along the axes.

B. Straight Line Constraint

Suppose the state of this system also satisfies the following linear equality constraint:

$$\mathbf{C}_k\mathbf{x}_k = \mathbf{d}_k, \tag{3}$$

where $\mathbf{C}_k$ is the constraint matrix with full row rank and $\mathbf{d}_k$ is the constraint vector. For example, if the following 2D road constraint is imposed on the system state:

$$\eta = a\xi + b, \tag{4}$$

which is specified by the slope a and intercept b, then dropping the index due to time invariance, the matrix form of the constraint in Eq. (3) can be written as

$$\mathbf{C}\mathbf{x}_k = \mathbf{d}, \tag{5}$$

where

$$\mathbf{C} = \begin{bmatrix} a & 0 & -1 & 0 \\ 0 & a & 0 & -1 \end{bmatrix}, \text{ and } \mathbf{d} = \begin{bmatrix} -b \\ 0 \end{bmatrix}. \tag{6}$$

If we denote $\mathbf{u}_k = [\mathbf{u}_{\xi,k} \quad \mathbf{u}_{\dot{\xi},k} \quad \mathbf{u}_{\eta,k} \quad \mathbf{u}_{\dot{\eta},k}]^T$, from Eq. (4), we have

$$\mathbf{u}_{\xi,k} = \frac{1}{a}\mathbf{u}_{\eta,k} \text{ and } \mathbf{u}_{\dot{\xi},k} = \frac{1}{a}\mathbf{u}_{\dot{\eta},k}, \tag{7}$$

and

$$\tilde{q}_\xi = \frac{1}{a^2}\tilde{q}_\eta. \tag{8}$$

Now, the process noise covariance becomes

$$\mathbf{Q} = \begin{bmatrix} \frac{\tilde{q}_\eta}{a^2} \begin{bmatrix} T^3/3 & T^2/2 \\ T^2/2 & T \end{bmatrix} & \frac{\tilde{q}_\eta}{a} \begin{bmatrix} T^3/3 & T^2/2 \\ T^2/2 & T \end{bmatrix} \\ \frac{\tilde{q}_\eta}{a} \begin{bmatrix} T^3/3 & T^2/2 \\ T^2/2 & T \end{bmatrix} & \tilde{q}_\eta \begin{bmatrix} T^3/3 & T^2/2 \\ T^2/2 & T \end{bmatrix} \end{bmatrix}. \tag{9}$$

C. Projection

The projection method projects the original unconstrained estimate (e.g., the output of a Kalman filter) onto the constraint surface by solving an optimization problem, usually by finding the point closest to the unconstrained estimate under a certain norm. This method is very easy to implement since it entails just one-step processing beyond the original unconstrained estimate[2].

In particular, suppose $\hat{\mathbf{x}}_k$ denotes an unconstrained estimate at time k. The constrained estimate $\hat{\mathbf{x}}_k^{proj}$ is found to be the solution of the optimization problem

$$\begin{aligned} \hat{\mathbf{x}}_k^{proj} &= \arg\min_{\hat{\mathbf{x}}_k} \|\mathbf{x}_k - \hat{\mathbf{x}}_k\|^2_{\mathbf{W}_k} \\ &\text{s.t. } \mathbf{C}_k\mathbf{x}_k = \mathbf{d}_k, \end{aligned} \tag{10}$$

for some symmetric and positive definite weight matrix $\mathbf{W}_k$, which can be then solved using the Lagrange multiplier method. The projected solution can be expressed as

$$\hat{\mathbf{x}}_k^{proj} = \hat{\mathbf{x}}_k + \mathbf{W}_k^{-1}\mathbf{C}_k^T(\mathbf{C}_k\mathbf{W}_k^{-1}\mathbf{C}_k^T)^{-1}(\mathbf{d}_k - \mathbf{C}_k\hat{\mathbf{x}}_k), \tag{11}$$

which provides a closed-form solution to project an unconstrained estimate onto the straight line constraint based on the general linear constraint Eq. (3). The weighting matrix $\mathbf{W}_k$ can be any user-supplied symmetric and positive-definite matrix of rank n (the size of the state space). Several proposed choices can be found in the literature, including the simplest identity matrix $\mathbf{I}$ [7], the (often) stable inverse process noise covariance matrix $\mathbf{Q}_k^{-1}$ [19], and the time-evolving inverse unconstrained error covariance $\mathbf{P}_k^{-1}$ [16].

III. NONLINEAR CONSTRAINED ESTIMATION AND PROJECTION

We extend the constrained estimation described in the previous section to more general nonlinear state models and constraints. We discuss both first- and second-order implementations of the projection method for circular trajectories.

A. Coordinated Turn (CT) Model

A maneuver (i.e., a turn) usually follows a pattern known as *coordinated turn* (CT) characterized by a near constant turn rate and near constant speeds along both coordinates. The turn rate Ω is accounted for by augmenting the state vector for our

[1]A superscript T always denotes the transpose of a vector or matrix.

[2]It is argued in [7] that the method itself is somewhat of a greedy approach where the solution may not guarantee the true constrained minimum.

2D motion model: $\mathbf{x} = \begin{bmatrix} \xi & \dot{\xi} & \eta & \dot{\eta} & \Omega \end{bmatrix}^T$, leading to the discretized CT model [2]:

$$\mathbf{x}_{k+1} = \begin{bmatrix} 1 & \frac{\sin \Omega_k T}{\Omega_k} & 0 & -\frac{1-\cos \Omega_k T}{\Omega_k} & 0 \\ 0 & \cos \Omega_k T & 0 & -\sin \Omega_k T & 0 \\ 0 & \frac{1-\cos \Omega_k T}{\Omega_k} & 1 & \frac{\sin \Omega_k T}{\Omega_k} & 0 \\ 0 & \sin \Omega_k T & 0 & \cos \Omega_k T & 0 \\ 0 & 0 & 0 & 0 & 1 \end{bmatrix} \mathbf{x}_k + \mathbf{u}_k, \quad (12)$$

and the covariance matrix of the process noise $\mathbf{u}_k$ is

$$\mathbf{Q}_k = \begin{bmatrix} \tilde{q}_\xi \begin{bmatrix} T^3/3 & T^2/2 \\ T^2/2 & T \end{bmatrix} & \mathbf{0}_{2\times 2} & \begin{matrix} 0 \\ 0 \end{matrix} \\ \mathbf{0}_{2\times 2} & \tilde{q}_\eta \begin{bmatrix} T^3/3 & T^2/2 \\ T^2/2 & T \end{bmatrix} & \begin{matrix} 0 \\ 0 \end{matrix} \\ \begin{matrix} 0 & 0 \end{matrix} & \begin{matrix} 0 & 0 \end{matrix} & \tilde{q}_\Omega T \end{bmatrix}, \quad (13)$$

where linear acceleration noise PSD levels in both dimensions are often assumed to be equal; i.e., $\tilde{q}_\xi = \tilde{q}_\eta$. The general guidelines for selecting appropriate levels of these noise parameters can be found in [2]. In contrast to the CWNA model, the CT model is nonlinear if the turn rate Ω is not a known constant, as can be seen from Eq. (12), where the state transition matrix contains the time-varying turn rate component.

B. Circular Constraint

Suppose the target trajectory satisfies the following circular constraint:

$$(\xi_k - \xi_c)^2 + (\eta_k - \eta_c)^2 = r^2, \quad (14)$$

where (ξ_c, η_c) is the center of the circle and r its radius. Now we let $\mathbf{p}_k = [\xi_k, \eta_k]^T$, $\mathbf{p}_c = [\xi_c, \eta_c]^T$, and $\mathbf{v}_k = [\dot{\xi}_k, \dot{\eta}_k]^T$. Then the constraint in Eq. (14) can be equivalently expressed as

$$(\mathbf{p}_k - \mathbf{p}_c)^T(\mathbf{p}_k - \mathbf{p}_c) = r^2, \quad (15)$$

and the constraint on the velocity is

$$(\mathbf{p}_k - \mathbf{p}_c)^T \mathbf{v}_k = 0. \quad (16)$$

To incorporate the circular constraint into the unconstrained CT model, a method is developed in [5] that utilizes the traveled distance s_k along the circular track and its change rate $\dot{s}_k$. More specifically, we have the state transition

$$\begin{bmatrix} \xi_{k+1} - \xi_c \\ \dot{\xi}_{k+1} \\ \eta_{k+1} - \eta_c \\ \dot{\eta}_{k+1} \end{bmatrix} = \mathbf{F}^c(\Omega_k T + \frac{w_k^s}{r}) \begin{bmatrix} \xi_k - \xi_c \\ \dot{\xi}_k - \frac{w_k^{\dot{s}}}{r}(\eta_k - \eta_c) \\ \eta_k - \eta_c \\ \dot{\eta}_k + \frac{w_k^{\dot{s}}}{r}(\xi_k - \xi_c) \end{bmatrix}, \quad (17)$$

where w_k^s and $w_k^{\dot{s}}$ are the process noise of s_k and $\dot{s}_k$ respectively and the matrix

$$\mathbf{F}^c(\Omega_k T + \frac{w_k^s}{r}) = \begin{bmatrix} \cos(\Omega_k T + \frac{w_k^s}{r})\mathbf{I}_{2\times 2} & -\sin(\Omega_k T + \frac{w_k^s}{r})\mathbf{I}_{2\times 2} \\ \sin(\Omega_k T + \frac{w_k^s}{r})\mathbf{I}_{2\times 2} & \cos(\Omega_k T + \frac{w_k^s}{r})\mathbf{I}_{2\times 2} \end{bmatrix} \quad (18)$$

contains the rotation element using the turning angle $\Omega_k T + \frac{w_k^s}{r}$. From Eq. (17), both position and velocity components at time $k+1$ are simply rotations of those at time k that is corrupted by noise. In addition, the updated turn rate component can be updated as

$$\Omega_{k+1} = \frac{\dot{\eta}_{k+1}}{\xi_{k+1} - \xi_c}. \quad (19)$$

C. Projection

We consider how to project an unconstrained estimate, e.g., one obtained via extended Kalman filter (EKF), onto the circular constraint.

1) First-Order Projection: Consider the circular constraint Eq. (15). We let

$$g(\mathbf{p}_k) = (\mathbf{p}_k - \mathbf{p}_c)^T(\mathbf{p}_k - \mathbf{p}_c) = r^2. \quad (20)$$

The first-order Taylor expansion of $g(\mathbf{p}_k)$ around $g(\hat{\mathbf{p}}_k^-)$ is

$$g(\mathbf{p}_k) \approx g(\hat{\mathbf{p}}_k^-) + g'(\hat{\mathbf{p}}_k^-)(\mathbf{p}_k - \hat{\mathbf{p}}_k^-) = r^2, \quad (21)$$

where $\hat{\mathbf{p}}_k^-$ is the unconstrained predicted position estimate at time k and

$$g(\hat{\mathbf{p}}_k^-) = (\hat{\mathbf{p}}_k^- - \mathbf{p}_c)^T(\hat{\mathbf{p}}_k^- - \mathbf{p}_c) \quad (22)$$

$$g'(\hat{\mathbf{p}}_k^-) = 2(\hat{\mathbf{p}}_k^- - \mathbf{p}_k)^T. \quad (23)$$

Rearranging the terms in Eq. (21), we have the following linear constraint:

$$g'(\hat{\mathbf{p}}_k^-)\mathbf{p}_k = r^2 - g(\hat{\mathbf{p}}_k^-) + g'(\hat{\mathbf{p}}_k^-)\hat{\mathbf{p}}_k^-. \quad (24)$$

Plugging Eqs. (22) and (23) into Eq. (24), and after some algebraic manipulation, we have

$$2(\hat{\mathbf{p}}_k^- - \mathbf{p}_c)^T \mathbf{p}_k = r^2 + (\hat{\mathbf{p}}_k^- - \mathbf{p}_c)^T(\hat{\mathbf{p}}_k^- + \mathbf{p}_c). \quad (25)$$

We can also express the above constraint in the matrix form:

$$\mathbf{C}_k \mathring{\mathbf{x}}_k = \mathbf{d}_k, \quad (26)$$

where $\mathring{\mathbf{x}}_k = [\xi_k, \dot{\xi}_k, \eta_k, \dot{\eta}_k]^T$ is the vector containing state position and velocity components (i.e.,without turn rate Ω_k), and

$$\mathbf{C}_k = \begin{bmatrix} a_k & 0 & b_k & 0 \\ 0 & a_k & 0 & b_k \end{bmatrix} \text{ and } \mathbf{d_k} = \begin{bmatrix} c_{1,k} \\ 0 \end{bmatrix} \quad (27)$$

are the constraint matrix and vector at time k respectively, where

$$a_k = \hat{\xi}_k^- - \xi_c, \quad (28)$$

$$b_k = \hat{\eta}_k^- - \eta_c, \quad (29)$$

$$c_{1,k} = (r^2 + (\hat{\xi}_k^-)^2 - \xi_c^2 + (\hat{\eta}_k^-)^2 - \eta_c^2)/2. \quad (30)$$

The linear projector of Eq. (11) can then be applied to the unconstrained estimate of $\mathring{\mathbf{x}}_k$ whereas the turn rate component Ω_k remains the same.

Alternatively, we can approximate the constraint on the position by using the predicted state components $\hat{\xi}_k^-$ and $\hat{\eta}_k^-$ directly:

$$\begin{bmatrix}\hat{\xi}_k^- - \xi_c & \hat{\eta}_k^- - \eta_c\end{bmatrix}\begin{bmatrix}\xi_k - \xi_c \\ \eta_k - \eta_c\end{bmatrix} = r^2, \tag{31}$$

which can then again be incorporated into the matrix format of Eq. (27) where $c_{1,k}$ in the constraint vector is replaced by $c_{2,k}$ such that

$$c_{2,k} = r^2 + (\hat{\xi}_k^- - \xi_c)\xi_c + (\hat{\eta}_k^- - \eta_c)\eta_c. \tag{32}$$

It can be shown that $c_{1,k} = c_{2,k}$ if and only if $(\hat{\xi}_k^- - \xi_c)^2 + (\hat{\eta}_k^- - \eta_c)^2 = r^2$, i.e., when the predicted estimate at time k happens to be located on the circular track.

2) Second-Order Projection: If the second-order Taylor expansion of $g(\mathbf{p}_k)$ around $g(\hat{\mathbf{p}}_k^-)$ is used, then constrained estimates can be found to be solution of a quadratic equation [15], which, in our circular track case, simply Eq. (20). In [20], a simple closed-form solution is provided which can be considered a "normalization" of the position estimate:

$$\hat{\mathbf{p}}_k^{proj} = \mathbf{p}_c + r\frac{\hat{\mathbf{p}}_k - \mathbf{p}_c}{\|\hat{\mathbf{p}}_k - \mathbf{p}_c\|}. \tag{33}$$

For a circular track, this simply means finding a point in the circle that is shortest distance to the unconstrained estimate.

Once this constrained position estimate is found, we can then use the the method similar to Eq. (31) to obtain the constrained velocity components. More specifically, the constraint on velocity now becomes

$$\begin{bmatrix}\hat{\xi}_k^{proj} - \xi_c & \hat{\eta}_k^{proj} - \eta_c\end{bmatrix}\begin{bmatrix}\dot{\xi}_k \\ \dot{\eta}_k\end{bmatrix} = 0, \tag{34}$$

which can be easily incorporated into the unconstrained estimate by the linear projection rule of Eq. (11). For example, if we use $\mathbf{W} = \mathbf{I}_{2\times 2}$, then the constrained velocity can be obtained as

$$\begin{aligned}
&\hat{\mathbf{v}}_k^{proj} = \\
&\hat{\mathbf{v}}_k - \frac{1}{\|\hat{\mathbf{p}}_k^{proj} - \mathbf{p}_c\|^2}\begin{bmatrix}\hat{\xi}_k^{proj} - \xi_c \\ \hat{\eta}_k^{proj} - \eta_c\end{bmatrix}\begin{bmatrix}\hat{\xi}_k^{proj} - \xi_c \\ \hat{\eta}_k^{proj} - \eta_c\end{bmatrix}^T \hat{\mathbf{v}}_k = \\
&\begin{bmatrix}(\hat{\eta}_k^{proj} - \eta_c)^2 & -(\hat{\xi}_k^{proj} - \xi_c)(\hat{\eta}_k^{proj} - \eta_c) \\ -(\hat{\xi}_k^{proj} - \xi_c)(\hat{\eta}_k^{proj} - \eta_c) & (\hat{\xi}_k^{proj} - \xi_c)^2\end{bmatrix}\frac{\hat{\mathbf{v}}_k}{r^2}.
\end{aligned} \tag{35}$$

IV. Fusion of Constrained Estimates

In this section, we first review conventional closed-form fusion rules (i.e., for unconstrained estimates), and then discuss ways to incorporate the constrained estimates into these rules. Without loss of generality, a two-sensor scenario is used through the rest of the paper since the results can be readily extended to cases involving more sensors.

A. Fusion Rules

1) Average Fuser: The simplest fuser is the average fuser, where the arithmetic mean of the sensor estimates is calculated as the fuser output:

$$\mathbf{P}_k^G = \frac{1}{2}(\mathbf{P}_k^1 + \mathbf{P}_k^2) \tag{36}$$

$$\hat{\mathbf{x}}_k^G = \frac{1}{2}(\hat{\mathbf{x}}_k^1 + \hat{\mathbf{x}}_k^2), \tag{37}$$

in which the superscript "G" denotes the the global estimate at the fusion center.

2) Simple Track-to-Track Fusion: The simple track-to-track fusion (T2TF) is performed by the fusion center as follows [2]:

$$(\mathbf{P}_k^G)^{-1} = (\mathbf{P}_k^1)^{-1} + (\mathbf{P}_k^2)^{-1} \tag{38}$$

$$\hat{\mathbf{x}}_k^G = \mathbf{P}_k^G\left((\mathbf{P}_k^1)^{-1}\hat{\mathbf{x}}_k^1 + (\mathbf{P}_k^2)^{-1}\hat{\mathbf{x}}_k^2\right). \tag{39}$$

It is well known that the common process noise results in correlation in the error cross-covariance across sensor estimates. However, it is generally difficult to derive the exact cross-covariances over time; as a result, one may assume that the cross-covariance is negligible in order to apply this simplified fuser, even though the result will be suboptimal.

3) Fast Covariance Intersection (CI) Algorithm: Another sensor fusion method without knowledge of the cross-covariance information is the covariance intersection (CI) algorithm. The method is characterized by the weighted convex combination of sensor covariances:

$$(\mathbf{P}_k^G)^{-1} = \omega_1(\mathbf{P}_k^1)^{-1} + \omega_2(\mathbf{P}_k^2)^{-1} \tag{40}$$

$$\hat{\mathbf{x}}_k^G = \mathbf{P}_k^G\left(\omega_1(\mathbf{P}_k^1)^{-1}\hat{\mathbf{x}}_k^1 + \omega_2(\mathbf{P}_k^2)^{-1}\hat{\mathbf{x}}_k^2\right), \tag{41}$$

where $\omega_1, \omega_2 > 0$ ($\omega_1 + \omega_2 = 1$) are weights to be determined (e.g., by minimizing the determinant of $\mathbf{P}_k^G$). A fast CI algorithm has been proposed in [17] where the weights are found based on an information-theoretic criterion so that ω_1 and ω_2 can be solved for analytically as follows:

$$\omega_1 = \frac{D(p_1, p_2)}{D(p_1, p_2) + D(p_2, p_1)}, \tag{42}$$

where $D(p_A, p_B)$ is the Kullback-Leibler (KL) divergence from $p_A(\cdot)$ to $p_B(\cdot)$, and $\omega_2 = 1 - \omega_1$. When the underlying estimates are Gaussian, the KL divergence at time k can be computed as

$$\begin{aligned}
&D_k(p_i, p_j) = \\
&\frac{1}{2}\left[\ln\frac{|\mathbf{P}_k^j|}{|\mathbf{P}_k^i|} + \mathbf{d}_{k,i\to j}^T(\mathbf{P}_k^j)^{-1}\mathbf{d}_{k,i\to j} + Tr(\mathbf{P}_k^i(\mathbf{P}_k^j)^{-1}) - n\right],
\end{aligned} \tag{43}$$

where $\mathbf{d}_{k,i\to j} = \hat{\mathbf{x}}_k^i - \hat{\mathbf{x}}_k^j$, n is the dimensionality of the state, and $|\cdot|$ denotes the determinant.

B. Fusion Rules with Constrained Estimates

While it may seem trivial to incorporate the one-step projection into the fuser, there are practical concerns regarding how to implement the projection. If the sensors do not perform projection themselves, i.e., the fuser inputs are all

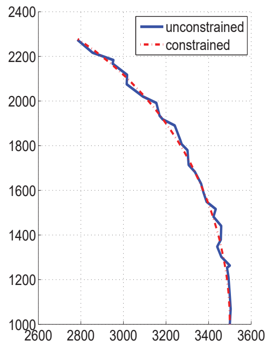

Fig. 1: Unconstrained and constrained position estimates

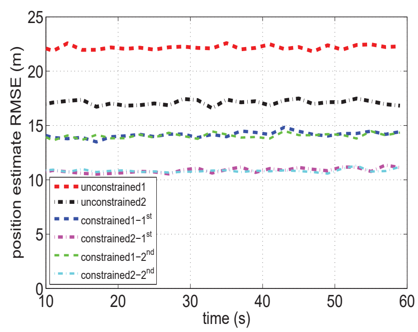

Fig. 2: Position RMSE of unconstrained and constrained estimates at each sensor

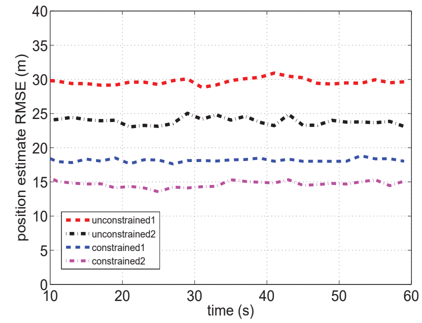

(a) 25% loss

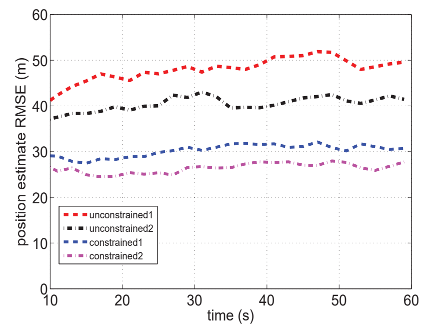

(b) 50% loss

Fig. 3: Position RMSE of sensor estimates at the fusion center

unconstrained estimates, then the fuser can simply perform conventional fusion, followed by one-step correction using first- or second-order projection methods described earlier, which can be considered "centralized projection". However, if one or more sensors send their self-projected estimates to the fusion center, as in "distributed projection", the latter cannot directly apply the T2TF, fast-CI, or any fusion rule that requires the inverse of the error covariances as the projected covariances are always singular. The sensors can, however, still send their unconstrained (nonsingular) covariances to the fusion center so that the latter can apply the T2TF and CI fusers.

V. Constrained Fusion with Information Loss

In this section, we present the position estimate root-mean-squared error (RMSE) performances of the constrained estimation and fusion methods described in previous sections by means of a tracking example. In particular, we consider the effect of information loss on constrained fusion performance under different fusion rules.

A. Simulation Setup

The center of the circular track is $(\xi_c, \eta_c) = (2000, 1000)$ m with a radius of $r = 1500$ m. A total of 5000 simulations are run for each test scenario. The initial state of the target is generated around $\mathbf{x}_0 = (\xi_c + r, \eta_c, 0, v_0, v_0/r)$ where $v_0 = 25$ m/s; that is, the initial position is centered around $(\xi_c + r, \eta_c)$ and the mean magnitude of the initial velocity is v_0. The target state is generated for a total of 60 seconds using the constrained target model presented in Section III-B.

Two sensors are used to observe the constrained motion where the (position) measurements are generated as

$$\mathbf{H}^{(1)} = \mathbf{H}^{(2)} = \begin{bmatrix} 1 & 0 & 0 & 0 & 0 \\ 0 & 0 & 1 & 0 & 0 \end{bmatrix}$$
$$\mathbf{V}^{(1)} = \text{diag}\{20^2, 20^2\} \quad \mathbf{V}^{(2)} = \text{diag}\{15^2, 15^2\},$$

where $\mathbf{H}$ and $\mathbf{V}$ are the measurement matrix and noise covariance respectively. Each sensor is initialized with a sufficiently large error covariance and runs EKF on top of the CT model with appropriate parameters, i.e., the process noise PSDs $\tilde{q}_\xi$, $\tilde{q}_\eta$, and $\tilde{q}_\Omega$ that reflect the level of process noise w_k^s in Eq. (18), the latter of which is generated here as a zero-mean normal random variable with a standard deviation of 5 m. The estimation interval is set to be $T = 2$ s.

B. Performance

1) Sensor Performance: We first examine the estimation performance of the individual sensors. Two modes of sensor configurations are considered, depending on whether a sensor incorporates the circular constraint Eq. (14). Fig. 1 shows the trajectories of both the original/unconstrained and constrained position estimates generated by Sensor 1 during one run of the simulation, where the first-order projection is used to project the unconstrained estimates onto the circle. The position RMSE performances at both sensors are plotted in Fig. 2 for

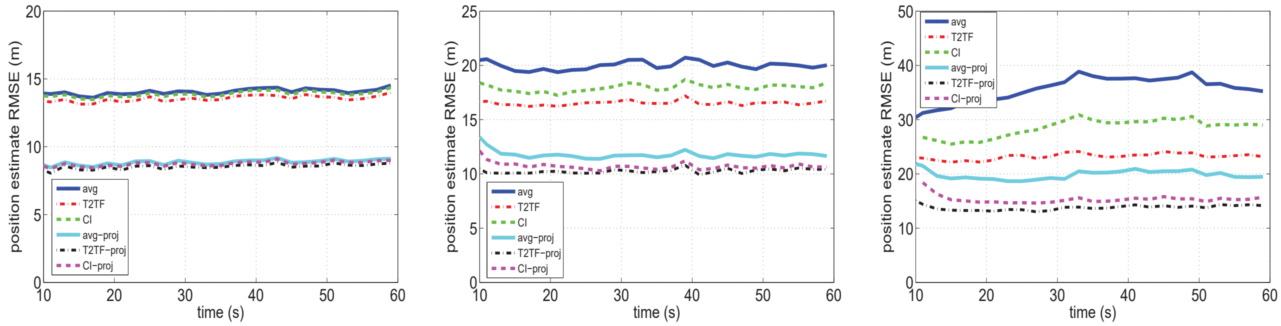

(a) 0% loss (b) 25% loss (c) 50% loss

Fig. 4: Position RMSE of fused estimates using unconstrained sensor estimates

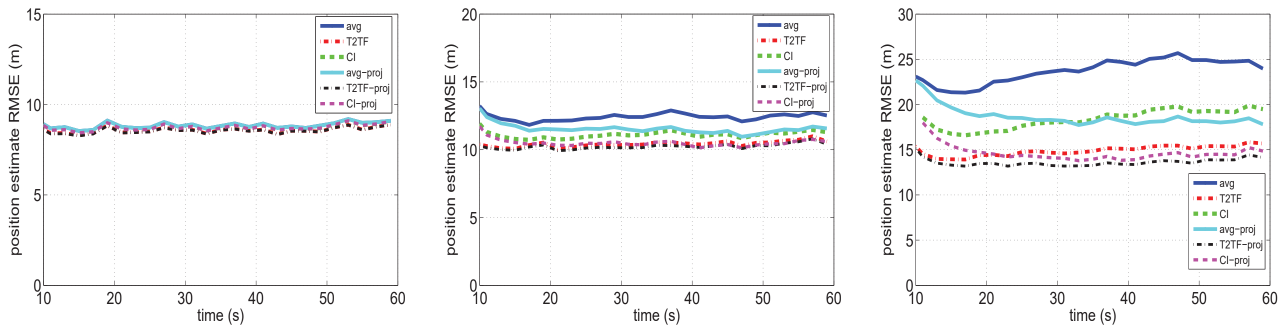

(a) 0% loss (b) 25% loss (c) 50% loss

Fig. 5: Position RMSE of fused estimates using constrained sensor estimates

both unconstrained and constrained (with first- and second-order projection) estimates. From the results, incorporating the constrained model can significantly improve the estimation accuracy performance at both sensors, where the position RMSEs can be reduced by approximately 40%. In addition, the difference in overall tracking performance using first-order versus second-order projection is negligible, with the desired benefit of much reduced computational overhead with the latter. In what follows, we will focus on the second-order solution with the understanding that it largely represents the performance of the first-order projection as well.

Before exploring the tracking performance at the fusion center, we want to first take a look at the effect of information loss on received sensor estimates at the fusion center. Communication loss can effectively reduce the number of successfully delivered estimates, whereupon the fusion center needs to apply prediction (using the same CT model) from the previously available estimates for a sensor and such predicted values would then be used as input for subsequent fusion. In Fig. 3, the position RMSEs of the sensor estimates used as fuser inputs are plotted for 25% and 50% link loss rates for both sensors. With 25% loss, the position RMSEs in Fig. 3(a) are variably 30-40% higher than their counterparts in Fig. 2, whereas those in Fig. 3(b) with 50% loss are more than twice their respective lossless RMSEs. In general, more prediction steps need to be carried out by the fuser with increasing link loss to fill in the missing estimates, thereby increasing the overall estimation errors, which would, in turn, inevitably lead to increased errors in the fused estimates as will be shown below.

2) Fuser Performance with Unconstrained Sensor Estimates: In Fig. 4, fusion performances under 0%, 25%, and 50% losses using unconstrained sensor estimates (from both sensors) are plotted. The notation "-proj" in the legend stands for FC-enabled projection after fusion of unconstrained estimates. From the plots, the errors of these constrained fused estimates are lower than their unconstrained counterparts; for example, for the simple track-to-track fuser (T2TF), consistently yielding the best performance followed by CI and average fusers, the reduction in position RMSEs is generally around 40%. Interestingly, the performance gaps among the fusers also increase significantly with higher link loss rates, demonstrating the advantage of the T2TF in its lower tracking errors and less sensitivity with respect to increased loss.

3) Fuser Performance with Constrained Sensor Estimates: Finally, we repeat the above simulations, but now with projected sensor estimates (and nonsingular unconstrained sensor error covariances) as the fuser input. From Fig. 5, we observe that without fuser projection, the position RMSEs are smaller than their counterparts in Fig. 4, thanks to the already improved estimates from the projection performed by the sensors themselves. On the other hand, if the fusion center does perform an additional correction step, then the resulting tracking errors are largely identical to their respective "-proj" cases in Fig. 4 with unconstrained sensor estimates.

4) Discussions: From the above results, information loss indeed results in increased tracking error across the board as expected. The fusion performances under such lossy conditions as shown in Figs. 4 and 5 all compare favorably to those of corresponding (received) sensor estimates in Fig. 3. It also appears to be more crucial for the fusion center to perform the final projection step, regardless of constrained/unconstrained nature of the individual sensor estimates. For example, for T2TF and CI fusers, even with 50% loss, the fusion center, after running projection, can still yield more accurate position estimates compared to the original unconstrained sensor estimates in Fig. 2.

In practice, the radial nature of the projection rule Eq. (33) would have the effect that the closer an unconstrained estimate is to the center, the higher the probability that it is projected to a point on the circle farther away from the ground truth, which can occur with increased sensor measurement variance and/or non-zero bias. As such, a sensor-projected estimate sent to the fusion center would lead to little insight for the latter to decide whether it should incorporate this particular estimate. From this perspective, it would seem more preferable to have the fusion center carry out the final-projection step, i.e., applying centralized projection, to reduce the overall uncertainty in sensor measurement quality.

VI. Conclusions

In this work, we studied constrained estimation and fusion performance where the target trajectory is bounded by a circular track constraint. The effect of information loss due to long-haul communications and the different ways to implement projection was also investigated, whereby we observed that final projection by the fusion center can most effectively improve the overall tracking performance under variable lossy conditions. Future extensions of this work include non-projection-based solutions for circular tracks and constrained fusion with other quadratic target motion constraints, e.g., those defined by elliptical tracks. More complex sensor measurement models that involve measurement bias may also be studied. Also of interest are scenarios with partially known and/or time-varying constraint parameters, for which a more adaptive multiple-model approach is needed to account for the increased uncertainty in the tracking system.

Acknowledgment

This work is funded by the Mathematics of Complex, Distributed, Interconnected Systems Program, Office of Advanced Computing Research, U.S. Department of Energy, and SensorNet Project of Office of Naval Research, and is performed at Oak Ridge National Laboratory managed by UT-Battelle, LLC for U.S. Department of Energy under Contract No. DE-AC05-00OR22725.

References

[1] I. F. Akyildiz, W. Su, Y. Sankarasubramaniam, and E. Cayirci. A survey on sensor networks. *Communications Magazine, IEEE*, 40(8):102–114, Aug. 2002.

[2] Y. Bar-Shalom, P. K. Willett, and X. Tian. *Tracking and Data Fusion: A Handbook of Algorithms*. YBS Publishing, 2011.

[3] W. Boord and J. B. Hoffman. *Air and Missile Defense Systems Engineering*. CRC Press, Boca Raton, FL, 2016.

[4] Z. Duan and X. R. Li. Constrained target motion modeling – part i: straight line track. In *Proc. 16th International Conference on Information Fusion (FUSION)*, pages 2161–2167, Istanbul, Turkey, Jul. 2013.

[5] Z. Duan and X. R. Li. Constrained target motion modeling – part ii: circular track. In *Proc. 16th International Conference on Information Fusion (FUSION)*, pages 2153–2160, Istanbul, Turkey, Jul. 2013.

[6] Z. Duan and X. R. Li. Multi-sensor estimation fusion for linear equality constrained dynamic systems. In *Proc. 16th International Conference on Information Fusion (FUSION)*, pages 93–100, Istanbul, Turkey, Jul. 2013.

[7] R. J. Hewett, M. T. Heath, M. D. Butala, and F. Kamalabadi. A robust null space method for linear equality constrained state estimation. *Signal Processing, IEEE Transactions on*, 58(8):3961–3971, Aug. 2010.

[8] Q. Liu, K. Brigham, and N. S. V. Rao. Estimation and fusion for tracking over long-haul links using artificial neural networks. *IEEE Transactions on Signal and Information Processing over Networks*, 3(3), Sep. 2017.

[9] Q. Liu and N. S. V. Rao. Projection-based linear constrained estimation and fusion over long-haul links. In *Proc. 12th International Conference on Multisensor Fusion and Integration for Intelligent Systems (MFI)*, pages 365–370, Baden-Baden, Germany, Sep. 2016.

[10] Q. Liu and N. S. V. Rao. State estimation and fusion over long-haul links under linear constraints. In *Proc. 19th International Conference on Information Fusion (FUSION)*, pages 1937–1944, Heidelberg, Germany, Jul. 2016.

[11] Q. Liu, N. S. V. Rao, and X. Wang. Staggered scheduling of sensor estimation and fusion for tracking over long-haul links. *IEEE Sensors Journal*, 16(15):6130–6141, Aug. 2016.

[12] Q. Liu, X. Wang, and N. S. V. Rao. Information feedback for estimation and fusion in long-haul sensor networks. In *Information Fusion (FUSION), 2014 17th International Conference on*, pages 1–8, Salamanca, Spain, Jul. 2014.

[13] Q. Liu, X. Wang, and N. S. V. Rao. Fusion of state estimates over long-haul sensor networks with random loss and delay. *Networking, IEEE/ACM Transactions on*, 23(2):644–656, Apr. 2015.

[14] Q. Liu, X. Wang, N. S. V. Rao, K. Brigham, and B. V. K. Vijaya Kumar. Effect of retransmission and retrodiction on estimation and fusion in long-haul sensor networks. *Networking, IEEE/ACM Transactions on*, 24(1):449–461, Feb. 2016.

[15] D. Simon. Kalman filtering with state constraints: a survey of linear and nonlinear algorithms. *Control Theory Applications, IET*, 4(8):1303–1318, Aug. 2010.

[16] D. Simon and T. L. Chia. Kalman filtering with state equality constraints. *Aerospace and Electronic Systems, IEEE Transactions on*, 38(1):128–136, Jan. 2002.

[17] Y. Wang and X. R. Li. Distributed estimation fusion with unavailable cross-correlation. *Aerospace and Electronic Systems, IEEE Transactions on*, 48(1):259–278, Jan. 2012.

[18] L. Xu, X. R. Li, Z. Duan, and J. Lan. Modeling and state estimation for dynamic systems with linear equality constraints. *Signal Processing, IEEE Transactions on*, 61(11):2927–2939, Jun. 2013.

[19] L. Xu, X. R. Li, Y. Liang, Z. Duan, and Q. Feng. An effective modeling framework for equality-constrained dynamic systems. In *Proc. 18th International Conference on Information Fusion (FUSION)*, pages 1868–1875, Washington, DC, Jul. 2015.

[20] C. Yang and E. Blasch. Kalman filtering with nonlinear state constraints. *Aerospace and Electronic Systems, IEEE Transactions on*, 45(1):70–84, Jan. 2009.